IEEE Transactions on Power Electronics, pp. 1–1, 2022

Resonant IGCT Soft-Switching: ZVS or ZCS

G. Ulissi, J. Kucka, U. Vemulapati, *et al.*

POWER ELECTRONICS LABORATORY
ÉCOLE POLYTECHNIQUE FÉDÉRALE DE LAUSANNE

This article has been accepted for publication in a future issue of this journal, but has not been fully edited. Content may change prior to final publication. Citation information: DOI 10.1109/TPEL.2022.3170114, IEEE Transactions on Power Electronics

Resonant IGCT Soft-Switching: ZVS or ZCS?

Gabriele Ulissi, *Graduate Student Member, IEEE*, Jakub Kucka, *Member, IEEE*, Umamaheswara Reddy Vemulapati, *Member, IEEE*, Thomas Stiasny, and Drazen Dujic, *Senior Member, IEEE*

***Abstract*—In the last thirty years the IGCT has been employed in medium voltage MW power level converters and has demonstrated some of the lowest conduction losses of any actively controlled device in traditional hard-switched, sub-kHz applications. Extending the use of the device to medium frequency applications such as DC transformers is possible through soft-switched operation, where low turn-off current and zero voltage turn-on significantly reduce switching losses. For this purpose, this paper explores the trade-offs in the transition between zero voltage and zero current switching conditions of reverse conducting IGCTs. Switching conditions resulting in minimal switching loss are identified for standard commercial devices and engineering samples subjected to increased electron irradiation to reduce switching energy at the expense of on-state voltage. The operation of the IGCTs at the record frequency of $5\,\mathrm{kHz}$ is thermally validated under load in the identified switching conditions.**

I. Introduction

Low-voltage (LV) and medium-voltage (MV) direct current (dc) distribution systems offer many advantages compared to their alternating current (ac) counterparts, thanks to their increased efficiency and lower operating costs. The absence of reactive power compensation and grid synchronisation requirements, simplicity in the integration of renewables, modern DC loads, and energy storage systems, further tip the scale in their favour [1]–[4]. For these reasons, low-voltage direct current (LVdc) distribution systems are already becoming the standard for applications such as shipboard power distribution networks and data centres, while applications of medium-voltage direct current (MVdc) systems are expected to increase in the coming years as standardisation and availability of suitable technologies increase [5]–[8]. In this context, the DC transformer (DCT) has been identified as a crucial enabling technology providing essentially the same function of isolation and interfacing of different voltage level buses that a traditional transformer provides in AC systems, as seen in Fig. 1. However, compared to traditional transformers, DCTs can additionally provide a significant reduction in size and weight of the device, which is an effective way to reduce costs through smaller system footprint, increased power density and reduced use of raw materials. This was achieved thanks to the capabilities of modern power semiconductors, with switching frequencies of several kHz having been demonstrated [9], [10].

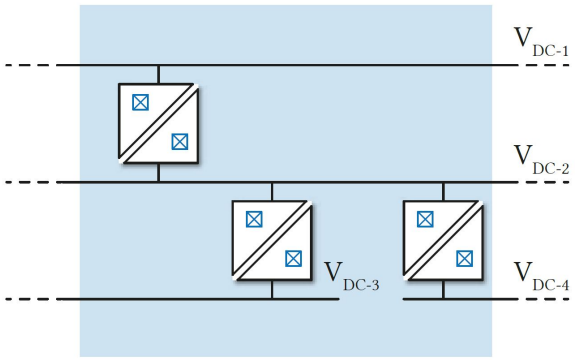

Fig. 1: DC transformers allow the interfacing of buses at different voltage levels without requiring active control of the power flow.

Thanks to the need for high frequency operation, the SiC MOSFET has been steadily gaining ground and attracting much research interest in high power DC conversion [11]–[13]. However, the prevailing semiconductor technology in this application is still the silicon insulated-gate bipolar transistor (IGBT), thanks to its wide availability, ruggedness, ease of drive and good switching characteristics [14]–[17]. The IGBT has found application in both dual active bridge (DAB) and series resonant converter (SRC) embodiments of dc transformers [18].

Over the past few decades and in other applications (such as MV drives), the integrated gate-commutated thyristor (IGCT) has emerged as an alternative device providing reliable performance at the MV level, with its use mainly being reserved to power levels above $1\,\mathrm{MW}$ and switching frequencies well below $1\,\mathrm{kHz}$ [19]–[23]. Compared to the more popular IGBT, the IGCT, being a thyristor-based device, benefits from lower conduction losses. Furthermore, it boasts improved reliability, larger safe operating area (SOA) and lower thermal resistance between junction and case in press-packed devices thanks to excellent utilisation of the silicon wafer area [23].

While soft-switched operation of the MOSFET and IGBT is well demonstrated, until [24] was presented, the use of IGCTs has been reserved for hard switched topologies. These have turn-off currents in the range of several kA, for which the device is optimised, with resonant converter topologies not being a target application. However, the very low conduction

Gabriele Ulissi, Jakub Kucka and Drazen Dujic are with the Power Electronics Laboratory, Ecole Polytechnique Fédérale de Lausanne (EPFL), 1015 Lausanne, Switzerland (e-mail: gabriele.ulissi@epfl.ch; jakub.kucka@epfl.ch; drazen.dujic@epfl.ch). Umamaheswara Vemulapati and Thomas Stiasny are with Hitachi ABB Power Grids, Semiconductors, 5600, Lenzburg, Switzerland (e-mail: umamaheswara.vemulapati@hitachi-powergrids.com; thomas.stiasny@hitachi-powergrids.com).

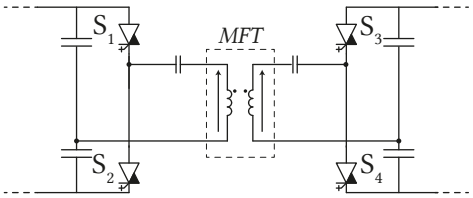

Fig. 2: Bidirectional half-bridge IGCT-based LLC-SRC topology with resonant capacitance distributed between primary and secondary. The topology can achieve high switching frequency through soft switching.

losses of the IGCT (second only to line-commutated thyristors) make it an interesting candidate for application in soft-switchd topologies, as this would combine its intrinsic excellent conduction characteristics with favourable zero voltage switching (ZVS) or zero current switching (ZCS) conditions in which such topologies operate. The reduction of switching and conduction losses provide leeway for the increase of the switching frequency, allowing the IGCT to reach frequencies of several kHz that are currently out of its ordinary operating range. Additionally, the use of a resonant topology allows the complete elimination of the clamp circuits that are required in hard-switched operation. This makes the IGCT a suitable candidate for DCT application in the LLC-SRC topology as in Fig. 2, which can be operated without closed loop control, relying on its stiff voltage transfer characteristic for power flow [25].

Nevertheless, this solution requires operation of the IGCT well beyond its common switching frequencies while maintaining safe operating conditions. To prove its feasibility, this paper analyses reverse-conducting IGCT (RC-IGCT) conduction and switching losses, identifying optimal, low-loss switching conditions by a comprehensive exploration of the ZVS/ZCS boundary of RC-IGCTs in resonant operation. Additionally, the paper demonstrates the operation of commercial $4.5\,\mathrm{kV}$ $68\,\mathrm{mm}$ RC-IGCTs at a frequency of $5\,\mathrm{kHz}$ and $2.5\,\mathrm{kV}$ dc link voltage in a test setup providing switching conditions equivalent to those of the LLC-SRC topology. Finally, engineering samples of RC-IGCT devices of the same ratings, optimised on the technology curve for reduced switching losses through increased levels of irradiation, are compared to commercial devices. As the switching losses in this operating mode will be shown in Section V to be prevalent over conduction losses, the faster state transition of devices with increased irradiation proves beneficial for the application in spite of the increased conduction loss.

The contributions of this paper are: *i)* the exploration and understanding of IGCT switching behaviour on the ZVS/ZCS boundary, exploring the underlying loss mechanism and including the effect of charge pre-flooding; *ii)* the evaluation of trade-offs resulting from varying levels of electron irradiation on IGCT loss minimisation in resonant applications.

This paper is organised as follows: Section II presents the tested semiconductor devices and the limitations of IGCT switching frequency, Section III discusses the employed test

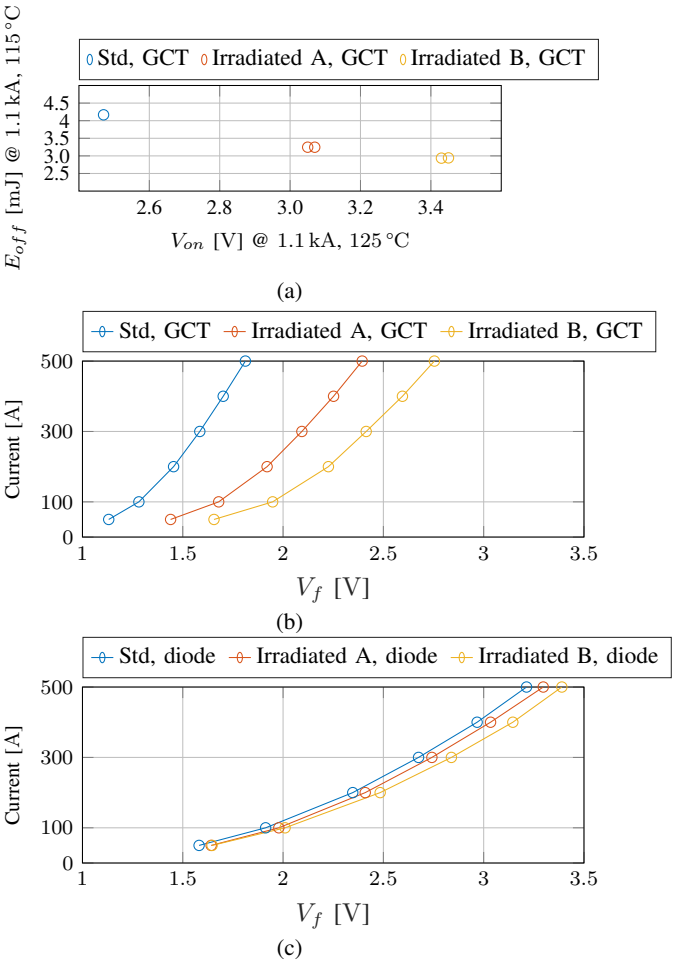

Fig. 3: a) Turn-off energy as a function of on-state voltage under hard switched conditions; b) GCT forward voltage, and c) diode forward voltage for ○ standard devices, ○ *Irradiated A*, and ○ *Irradiated B*.

setup with which experimental results are gathered, Section IV identifies the trade-offs and behaviour of RC-IGCTs switching at ultra-low (<20 A) turn-off current. Section V discusses conduction losses of standard and irradiated devices in the target DCT application, and finally Section VI verifies the feasibility of IGCT $5\,\mathrm{kHz}$ operation through thermal runs in steady state.

II. IGCT Switching Frequency Limitations and Devices

The IGCT has traditionally found application in hard-switched topologies operated at low (<kHz) frequencies. In these applications, the limitations that prevent an increase of switching frequency for the device (>1 kHz) can be synthesized as:

1) Turn-off switching losses: In high switching frequency applications (>1 kHz), relatively high E_{off} causes the device to exceed its operating junction temperature (thermal limitation).

2) Minimum turn-on time requirement of the device: it is required to have a minimum t_{on} time (typically >40 µs) to make sure that the device is turned *ON* homogeneously throughout the wafer before turn-off is initiated.
3) Minimum transient time requirement of the clamp circuit: a certain minimum time is required (> 10 µs) between switching transients to make sure that the clamp capacitor is discharged, and clamp diode is turned-off completely.

In particular, the minimum 40 µs *ON* time of the device is due to the need to achieve uniform current distribution in the device wafer before turn-off can be safely performed. The soft switching conditions presented in this paper overcome all the above limitations of the device:

1) E_{off} is very low as the turn-off occurs at ultra low currents, below 20 A (in first approximation, E_{off} changes linearly with the current).
2) No minimum turn-on time is required as the turn-off occurs at ultra low currents, therefore resulting in low localised energy density and no thermal hotspots on the wafer (does not have an impact on turn-off SOA).
3) No requirement of minimum transient time as the clamp circuit can be completely removed in the LLC-SRC topology.

In this paper, three devices are discussed: a commercially available 4.5 kV, 68 mm RC-IGCT device, and two custom engineering samples. The three design variants differ by the homogeneous lifetime control achieved through electron irradiation. The reference device is the commercial device with standard electron irradiation. This design is optimized for typical hard-switched, sub kHz applications. Devices referred to as *Irradiated A* and *Irradiated B* are subjected to higher electron irradiation to increase the switching speed and to be used in high frequency applications. These devices have 55 % and 95 % higher irradiation than the commercial devices (standard irradiated devices), respectively.

The technology trade-off of these three designs (RC-IGCTs with standard irradiation, *irradiated A* and *irradiated B*) are compared under hard-switched conditions (i.e. at high turn-off current and high dc-link voltage) using classical half bridge test configuration with clamp circuit. As shown in Fig. 3a, the increased irradiation reduces the turn-off energy losses at at turn-off current of 1.1 kA by 22 % and 29 % in *irradiated A* and *irradiated B*, respectively. However, the on-state voltage at the same current level of 1.1 kA increases by 23 % and 39 % in *irradiated A* and *irradiated B*, respectively, compared to standard irradiated devices. The improvement in switching performance with higher irradiation (*irradiated B*) has a larger trade-off on the on-state under hard-switched conditions.

However, as the focus of this work is LLC-SRC application, the performance has to be evaluated under soft-switched operation. The three designs are tested under these conditions (at turn-off currents below 20 A) using test setup shown in Fig. 4 and the results are presented in Section IV.

III. Test Setup

The IGCT test setup presented in [24] and displayed in Fig. 4a is used to gather the experimental results presented in this paper. The setup is wired as displayed in Fig. 4b, and emulates the behaviour of an LLC-SRC from the perspective of the semiconductor devices by subjecting them to voltage and current stresses equivalent to those of a full converter. The values of the components of the setup are listed in Table I.

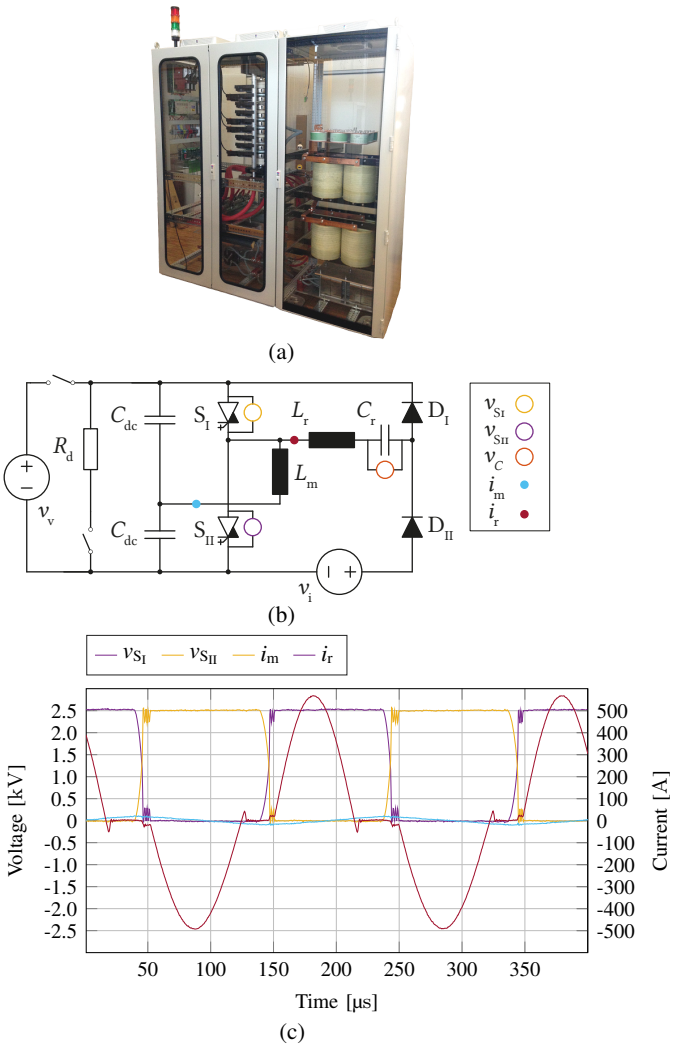

Fig. 4: a) The IGCT flexible test setup [26] is configured to emulate the behaviour of an LLC-SRC converter, as shown in b). Typical waveforms for the setup in this configuration are seen in c).

The setup waveforms in this configurations are shown in Fig. 4c. The setup is capable of circulating energy from the DC link capacitors C_{dc} into the IGCTs and resonant tank, and back into the capacitors through the diode rectifier. This is achieved by applying a voltage v_i to the return path of the current emulating a controllable load by creating an artificial

TABLE I: Components of the test setup.

V_v	V_i	C_{dc}	C_r	L_m	L_r
2.5 kV	0 V...20 V	2.6 mF	85 µF	1.5 mH...100 mH	8 µH

This article has been accepted for publication in a future issue of this journal, but has not been fully edited. Content may change prior to final publication. Citation information: DOI 10.1109/TPEL.2022.3170114, IEEE Transactions on Power Electronics

voltage difference between the resonant tank input and output. The voltage generated by v_{i} is modified to increase or decrease the value of the load current i_{r}, effectively simulating load variation in an LLC-SRC. The current i_{m} emulates the transformer magnetising current and is determined by the DC link voltage and the value of inductor L_{m}. The IGCTs conduct the sum of currents i_r and i_m. i_{r} is conducted for the duration of the resonant pulse, which is determined by the resonant frequency resulting from the values of C_{r} and L_{m}. It transfers power from the primary to the secondary side of the setup (or converter, in a real application). i_{m} is conducted throughout the period, and is necessary to maintain soft-switching conditions by forward-biasing the IGCT antiparallel diode before turn-on. Together, these two current recreate the advantageous conditions of low turn-off current and ZVS or ZCS turn-on present in the LLC topology.

IV. IGCT SWITCHING LOSSES AT ULTRA-LOW TURN-OFF CURRENT

An important benefit of the use of the resonant LLC-SRC topology is the low switching losses generated at turn-off (low current) and negligible losses at turn-on (ZVS). In hard switched applications and for high turn-off current levels, the turn-off losses of the IGCT are proportional to the turn-off current. Therefore, the lower the turn-off current, the more advantageous the turn-off conditions for the device. Nevertheless, when reducing the level of turn-off current (<100 A), [24] has shown how the duration of the transition of the IGCT from the *ON* state to the *OFF* state is significantly increased. For the purpose of minimising switching losses, it is essential to understand if and how very low values of turn-off current result in a switching transition slow enough to exceed the dead-time (also referred to as interlock time, or blanking time). If this is the case, partial shoot-through will result. How this affects IGCT switching losses must be explored.

A. Understanding the ZVS/ZCS transition

To explore the boundary between ZVS low-current turn-off and partial shoot-though, the test setup in Fig. 4 was configured with a very large value of magnetising inductance $L_m = 100\,\mathrm{mH}$, and a power supply voltage $V_i = 0\,\mathrm{V}$ (effectively the same behaviour as if the resonant tank was disconnected). In this configuration, the turn-on of IGCT $\mathrm{S_I}$ causes a linear increase of the magnetising current i_m up to the desired turn-off level. $\mathrm{S_I}$ is then turned *OFF* and after dead-time T_{dt} has passed, $\mathrm{S_{II}}$ is turned *ON*. The current and voltage waveforms of $\mathrm{S_I}$ are sensed, allowing to observe the switching waveforms as a function of the turn-off current. It is also possible to turn IGCT $\mathrm{S_{II}}$ *ON* first, and evaluate the turn-on waveforms of $\mathrm{S_I}$. As there is no resonant current flowing in the setup, the value of elements L_r and C_r is not relevant. The value of the DC link voltage V_v is set to 2500 V.

Fig. 5 displays turn-off and turn-on transitions for S_I, with various ultra-low (<20 A) values of switching current: 17 A, 9 A, and 0 A. In the LLC-SRC topology, the turn-off current value is equal to the peak magnetising current value in the transformer, while in the test setup in Fig. 4 to i_m. For all

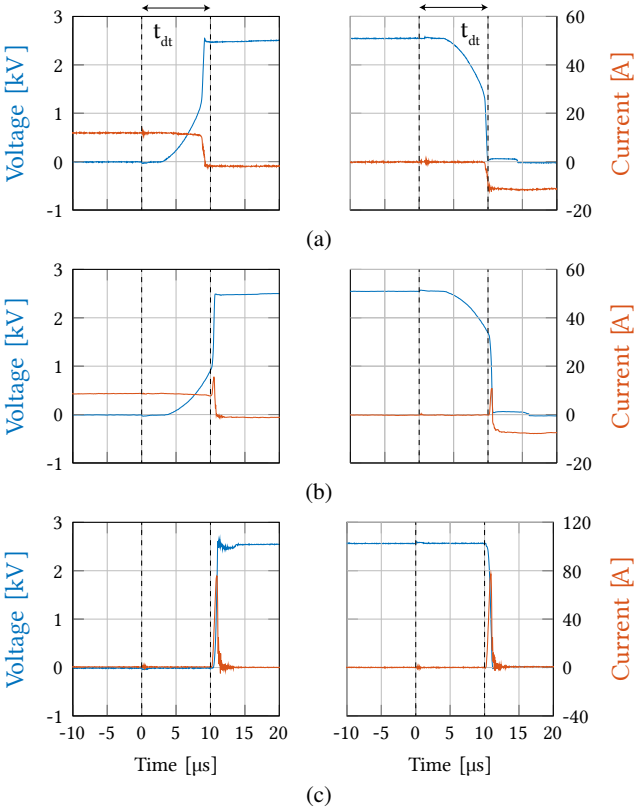

Fig. 5: Experimental IGCT waveforms displaying turn-off and turn-on under a) ZVS, b) non-ZVS, and c) zero-current conditions. The turn-off current values are 17 A, 9 A, and 0 A, respectively. With loss of ZVS partial shoot-though takes place due to incomplete n-base sweep-out.

three subfigures, switching waveforms are presented with the same dead-time of 10 µs. There are three different possible conditions that are presented: in Fig. 5a, the state transition of $\mathrm{S_I}$ happens in ZVS conditions. That is to say, the turn-off current level is sufficiently high to sweep out the n-base of $\mathrm{S_I}$ before the dead-time ends and $\mathrm{S_{II}}$ is turned *ON* (and vice-versa for turn-on). Fig. 5b displays the effect of a lower value of turn-off current (9 A). In such a condition, the current level is insufficient to complete the n-base sweep-out during the dead-time, and at the time of turn-on of $\mathrm{S_{II}}$, the turn-off of $\mathrm{S_I}$ is still incomplete. As $\mathrm{S_{II}}$ turns *ON*, a partial shoot-through takes place in both devices, as they briefly are both in conduction at the same time, since $\mathrm{S_I}$ is not completely turned *OFF* yet. This causes a current peak in both devices, and an increase in the amount of charge conducted through $\mathrm{S_{II}}$ during its turn-off. The partial shoot-through causes an increase in both turn-off losses for $\mathrm{S_I}$, and turn-on losses for $\mathrm{S_{II}}$. Finally, the complete disconnection of inductor L_m allows the evaluation of the effect of a turn-off current i_m = 0 A. This is not realistic in a true LLC-SRC topology, as the transformer magnetising inductance is a finite value, but it is of interest to evaluate the effect of a turn-off current level approaching 0 A.

Fig. 5c shows the switching transition under these conditions. The turn-off of $\mathrm{S_I}$ does not start as the device is turned

This article has been accepted for publication in a future issue of this journal, but has not been fully edited. Content may change prior to final publication. Citation information: DOI 10.1109/TPEL.2022.3170114, IEEE Transactions on Power Electronics

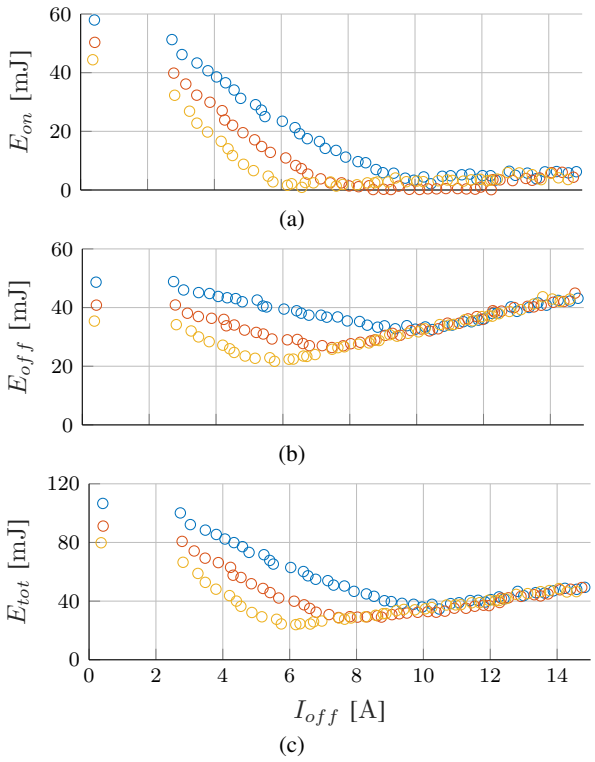

Fig. 6: a) Turn-on, b) turn-off, and c) total switching energy for standard commercial RC-IGCTs with dead-times of ○ 10 µs, ○ 12 µs, and ○ 14 µs.

OFF, as there is no current present in the device to clear charge carriers from the n-base. Instead, the state transition takes place only as S_{II} is turned *ON*. This results again in partial shoot-through, but the amount of charge that must be swept out of S_I is larger in this scenario, resulting in an increased current peak and consequently increased losses in both devices. Therefore, it is expected that the turn-off current resulting in the minimum switching losses is the minimum current level that allows the full transition of the IGCT during the dead-time. If the dead-time is longer, then a lower level of turn-off current can be used, while if the dead-time is shorter, then a larger turn-off current will be required to complete the sweep-out in the required time (assuming the turn-off current is a degree of freedom during design).

Thanks to the high values of the magnetising inductor in the test setup, the turn-off current can be carefully set by changing the *ON* time of S_I (or S_{II} for turn-on). Fig. 6 displays the turn-on and turn-off losses in the standard commercial RC-IGCTs as a function of turn-off current and dead-time (the leftmost part of the plot is not populated due to limitations on the available L_m and GCT minimum turn-on time). The exhibited trends are coherent with the expected results based on Fig. 5. Fig. 6a shows how turn-on loss is absent as long as ZVS conditions are maintained. Once ZVS conditions are lost, partial shoot-through takes place resulting in turn-on loss: as the turn-off current is reduced, there is an increasing amount of charge that is swept-out of the junction as the complementary device is turned *ON*. This results in progressively increasing losses up to the limit case of turn-off current equal to 0 A. The longer the dead-time, the lower the turn-off current can be while still maintaining ZVS. Fig. 6b shows how the turn-on loss is almost linear with the value of turn-off current when in ZVS conditions. Once ZVS is lost (to the left of the minimum), turn-off loss also increases due to partial shoot-through, as the resulting current spikes take place both during turn-on and turn-off. Finally, Fig. 6c displays the total switching loss. The figure clearly shows how, as expected, the minimum total switching loss happens at the minimum value of turn-off current which guarantees ZVS. This value increases with shorter dead-time, resulting in increased minimum switching loss, and conversely decreases with longer values of dead-time.

Applications which can allow extended duration of the dead-time can benefit from lower total switching loss. It is also observed that loss of ZVS, while resulting in increased loss, has a progressive effect. There is no remarkable increase in switching loss in the vicinity of the operating point where ZVS conditions are lost. Operation close to the optimal point will still result in relatively low switching loss, even if not in ZVS conditions.

B. Effect of pre-flooding and Irradiation

The test results gathered and displayed in Fig. 6 have determined that the optimal turn-off current level for switching loss minimisation is the minimum current that will guarantee ZVS conditions. However, during this phase of testing, the maximum current conducted by the device under test never exceeds the turn-off current level, which is very low. This is not representative of the operating conditions in an LLC-SRC converter, where the resonant current peak can be orders of magnitude larger than the turn-off current value. In conducting a significant current level, the IGCT is pre-flooded with charge carriers which increase the charge to be swept out upon turn-off, affecting the duration of the state transition. Consequently, this affects ZVS conditions, as more time is required to turn *OFF* the device at the same turn-off current level. Therefore, additional tests are carried out to quantify the effect of current pre-flooding. Here, devices *Irradiated A* and *Irradiated B* are additionally considered, as their reduced carrier lifetime will be shown to offer additional benefits during state transitions.

Fig. 7 displays the turn-on and turn-off energy of standard commercial RC-IGCTs and devices with increased irradiation levels as a function of peak conducted resonant current and turn-off current. The dead-time is set to 14 µs and is not changed throughout the experiments, as it is considered suitable for the application. The resonant frequency of the test setup resonant tank is set to 7.35 kHz and the voltage V_i is altered throughout the test to obtained the desired resonant current peak. V_v is kept at 2.5 kV.

The top row of Fig. 7 displays the IGCT turn-on energy. In ZCS conditions (L_m inductor disconnected, $I_{off} = 0$ A), turn-on losses are present for all three devices, which is expected since ZVS cannot be achieved. With an increase of the device's turn-off current, standard devices and both *Irradiated A* and *Irradiated B* devices exhibit different behaviours. Standard devices do not achieve ZVS switching over the whole range of

This article has been accepted for publication in a future issue of this journal, but has not been fully edited. Content may change prior to final publication. Citation information: DOI 10.1109/TPEL.2022.3170114, IEEE Transactions on Power Electronics

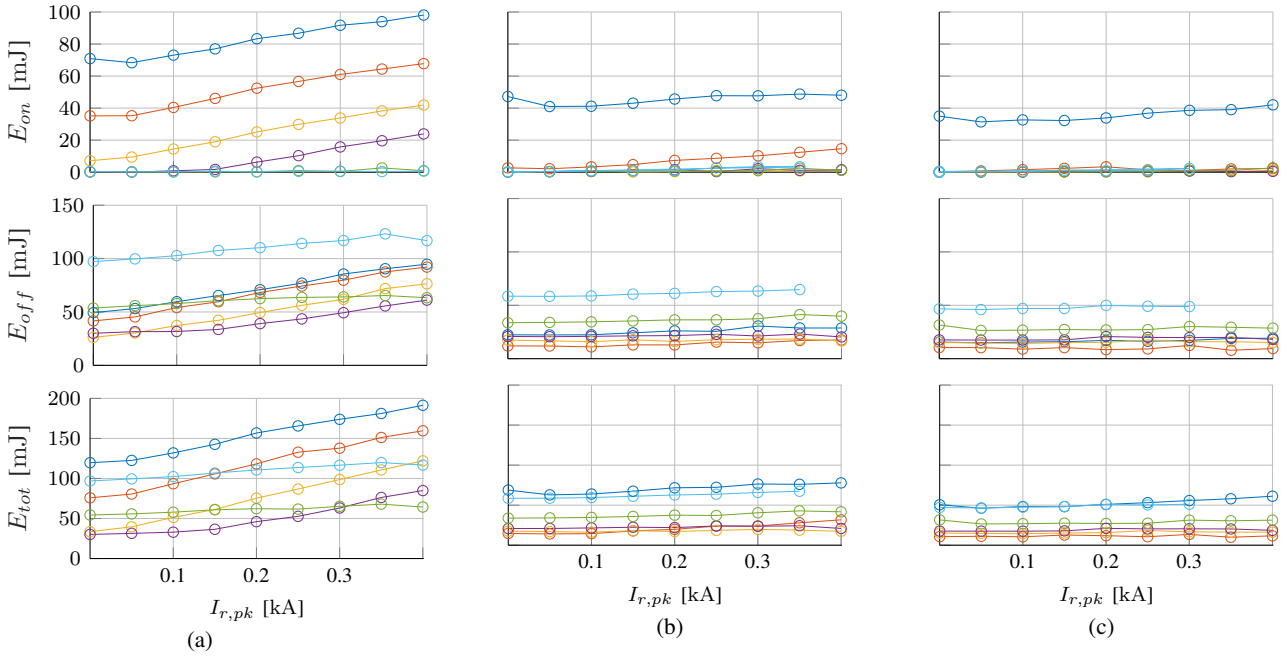

Fig. 7: Turn-on, turn-off, and total switching energy for a) standard commercial RC-IGCTs, b) *Irradiated A*, and c) *Irradiated B* devices. The duration of the dead-time is 14 µs and the turn-off current levels are of ○ 0 A, ○ 3 A, ○ 6 A, ○ 9 A, ○ 17 A, and ○ 34 A.

resonant peak current $I_{r,pk}$ until a turn-off current level of 17 A is reached. A lower current level of 9 A is only sufficient to maintain ZVS conditions up to 200 A of peak resonant current, resulting in turn-on losses being constant and equal to 0 mJ up to this level. The required 17 A are significantly higher than the turn-off current of 6 A, which was sufficient without pre-flooding. The turn-on energy of *Irradiated A* and *Irradiated B* devices is significantly lower than that of the standard device, even in ZCS conditions with I_{off} = 0 A. Additionally, due to a faster turn-off and turn-on state transition, a turn-off current of 6 A is sufficient to maintain ZVS conditions over the whole operating range for *Irradiated A*, while a turn-off current as low as 3 A is sufficient for *Irradiated B*. This can be concluded by the absence of turn-on losses at these current levels, signalling operation in ZVS conditions.

Coherently with their faster state transitions, increased irradiation devices also exhibit lower turn-off losses than standard devices, at the same turn-off current level. The turn-off energy of the *Irradiated B* is as low as half of that of the commercial device, for an equivalent turn-off current level. Also, the turn-off energy of all three devices exhibits different trends depending on whether the switching process occurs in ZVS conditions or not. In ZVS switching conditions, the turn-off energy of the device is almost invariant over the whole operating range. In contrast, if ZVS conditions are not met, the device turn-off energy increases linearly with the peak resonant current level, as the turn-off time increasingly exceeds the dead-time of 14 µs.

The total switching energy is therefore a sum of the discussed effect on the turn-on and turn-off energy. In the absence of ZVS, the total switching energy increases with $I_{r,pk}$, but in ZVS conditions, it stays constant over the operating range. To select the appropriate value of turn-off current for each device, the worst-case loss condition is considered. For all three devices, the larger the peak resonant current, the larger are both conduction (evaluated later) and switching losses. Therefore, the selected turn-off current level is the value of I_{off} for which the total switching losses at the maximum evaluated level of resonant current are the lowest. That is to say the minimum value of turn-off current which guarantees ZVS over the whole operating range. For standards devices, this level is 17 A, for *Irradiated A* devices 6 A, and for *Irradiated B* devices, 3 A.

This highlights how the advantage offered by devices subjected to increased electron irradiation is compounded in the context of switching loss. The devices have lower carrier lifetime, resulting in faster switching transitions and therefore reduced switching losses. But additionally, the faster switching transitions allow a reduction in turn-off current while still maintaining ZVS conditions, offering the additional benefit of not only guaranteeing reduced switching losses at a fixed current level, but a decrease of the optimal turn-off current and further reduced losses as a consequence.

V. Losses in Target Application

Having evaluated the switching losses of standard, *Irradiated A*, and *Irradiated B* devices, the conduction losses can be evaluated at different operating points.

The forward voltage of both RC-IGCTs and their antiparallel diodes are not evaluated in resonant operation, but by circulating a varying level of DC current through the device. Precision multimeters are employed for this task. The results

This article has been accepted for publication in a future issue of this journal, but has not been fully edited. Content may change prior to final publication. Citation information: DOI 10.1109/TPEL.2022.3170114, IEEE Transactions on Power Electronics

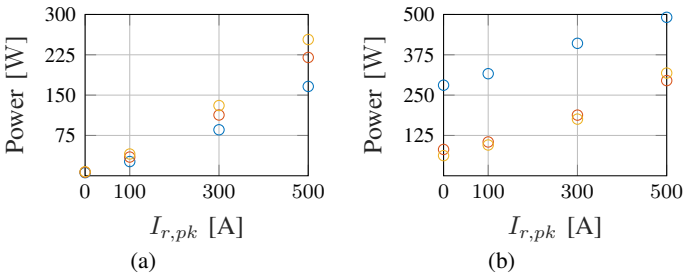

Fig. 8: Loss breakdown comparing conduction loss a) and total loss b) during 5 kHz operating with the computed ideal turn-off current value for ○ standard commercial devices, ○ *Irradiated A* devices, and ○ *Irradiated B* devices.

of the measurement are displayed in Fig. 3b. As expected, the higher irradiation level devices exhibit higher forward voltage at all current levels, both for the GCT and the antiparallel diode. By combining the devices' forward characteristic with current waveforms recorded in 5 kHz resonant operation, the conduction losses of each device can be calculated. Fig. 8 displays the loss breakdown in this operating mode. Fig. 8a shows that, as expected, conduction losses increase with the irradiation level of the device and with the peak resonant current level. For low resonant current levels (low load), a higher level of irradiation is advantageous, as it results in lowered switching losses, while conduction losses remain low due to the low current peak level. The opposite is also true, in that with high resonant current levels (high load), a lower level of irradiation is beneficial as increased switching losses are offset by an advantage in conduction loss.

In Fig. 8b the sum of the total calculated conduction and switching loss for the three devices is presented. For all three devices, the minimum turn-off current level guaranteeing ZVS conditions is considered to evaluate the switching loss (3 A, 6 A, and 17 A for standard, *Irradiated A*, and *Irradiated B* devices, respectively). Note that the total losses of the standard devices are significantly larger than the corresponding losses of higher irradiation samples over all the considered peak resonant current range. It can be then concluded that for the considered load levels, *Irradiated A* and *Irradiated B* devices are preferable. Nevertheless, it should be noted that already at a peak resonant current of 500 A, the total losses of device *Irradiated A* (lower irradiation) are lower than those of device *Irradiated B* (higher irradiation), as conduction losses become more prevalent with the increase of circulated current. As previously discussed, the available laboratory equipment did not allow the testing of higher resonant current operating points. Based on the gathered results, it is expected that for increasing test setup loads, devices with lower irradiation levels will result more favourable, as conduction losses progressively become a significant component of overall loss as the IGCTs operate closer to their rated current level. It is estimated that a peak resonant current of 2.3 kA would result in the total losses of standard commercial devices being lower than those of *Irradiated B*. While this current level exceeds the capabilities of the device, the principle remains

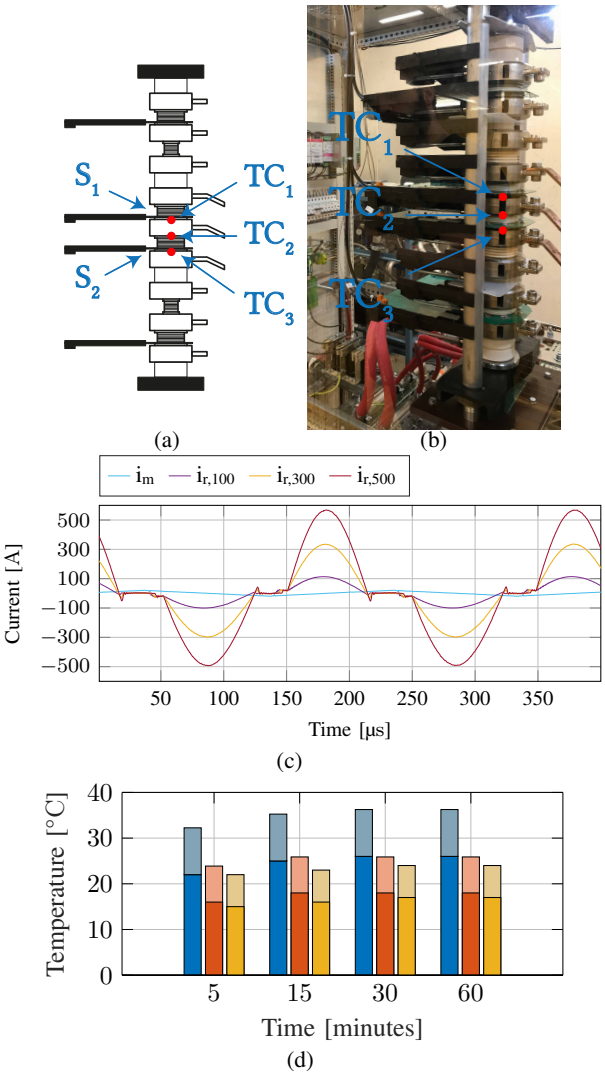

Fig. 9: a) Simplified drawing of the IGCT setup stack. Only the central two reverse conducting IGCTs are in use. The position of the thermocouples is displayed in the drawing and in the photo in b). The current waveforms recorded during 5 kHz operation are displayed in c), while the sensed IGCT case temperature (dark bar) and corresponding estimated junction temperature (light bar) is show in d) for ○ standard commercial devices, ○ *Irradiated A* devices, and ○ *Irradiated B* devices.

that depending on application at hand (in terms of switching frequency and nominal load) a device with a different level of electron irradiation may be selected. Higher irradiation results in more efficient operation at low load, when switching losses are prevalent, and vice-versa.

VI. Steady-State 5 kHz Operation

Finally, to prove the feasibility of high-frequency IGCT-based resonant DCT, hour-long thermal runs of the test setup were performed to evaluate the devices' junction temperatures during operation. The device case temperature was sensed through radio thermocouples inserted in grooves in the heatsink, allowing the thermocouple to reach and sense the

devices' case temperature. Figs. 9a and 9b show the location of the thermocouples. For steady-state operation, the turn-off current level is set to 17 A for all three tested devices due to thermal limitations of the available equipment. This turn-off current level is near ideal for the standard devices, but larger than needed for both *Irradiated A* and *Irradiated B*. The sensed case temperature and computed junction temperature for all three devices during thermals runs is displayed in Fig. 9d. For all three devices, the peak resonant current level is of 300 A, which is the value employed for the estimation of the junction temperatures, based on the datasheet case-to-junction thermal resistance of $25\,\frac{\mathrm{K}}{\mathrm{kW}}$. The estimated losses of the devices at this operating point are of 410 W, 315 W, and 280 W for standard devices, *Irradiated A*, and *Irradiated B*, respectively. The temperature of the deionised water circulated by the water cooling unit (WCU) is kept at only 10 °C, thanks to the heat exchange with the very cold water from lake Geneva, which is available in the laboratory. While such a low cooling water temperature is unrealistic for industrial applications, it nevertheless allows to observe the junction temperature gain over that of the WCU deionised water. Fig. 9d shows how a thermal steady state is reached in only 15 minutes, and how even for standard commercial devices there exists a very significant margin to the junction thermal limit of 115 °C. Neglecting the effect of increased junction temperature on semiconductor losses, in first approximation it is estimated that a WCU temperature of up to 70 °C is likely to be acceptable for standard devices. Higher values can be tolerated by increased irradiation devices thanks to their overall lower losses at this operating point.

VII. Conclusion

This paper has examined the the switching behaviour of RC-IGCTs at ultra-low (<20 A) turn-off current, considering standard commercial devices and custom engineering samples subjected to increased levels of electron irradiation. It is concluded that an optimal turn-off current level exists at the threshold of ZVS conditions, and that said threshold is affected both by dead-time duration and semiconductor pre-flooding. Larger values of conducted current result in slower IGCT turn-off, resulting in loss of ZVS with turn-off current levels which ensure ZVS at no-load operation. Notably, the loss of ZVS conditions is found to increase switching loss, but the increase of losses is progressive and not immediately destructive for the IGCTs. Devices subjected to higher levels of irradiation present reduced switching losses due both to their faster turn-off, and to the lower values of turn-off current that can be used while still maintaining ZVS conditions. The limitations of these devices emerge as converter load becomes very high, and increased levels of irradiation ultimately result in increased loss due to the higher forward voltage during conduction. 5 kHz operation of RC-IGCTs is demonstrated to be feasible with safe estimated junction temperatures. In summary, the ZVS mode of operation with sufficiently low turn-off current is preferred over ZCS, for the DCT topology considered in the paper.

VIII. Acknowledgements

The results presented in this paper are a part of the EM-POWER project that has received funding from the European Research Council (ERC) under the European Union's Horizon 2020 research and innovation programme (Grant agreement No. 818706).

References

[1] S. Cui, N. Soltau, and R. W. De Doncker, "A high step-up ratio soft-switching dcdc converter for interconnection of mvdc and hvdc grids," *IEEE Transactions on Power Electronics*, vol. 33, no. 4, pp. 2986–3001, 2018.

[2] L. Zhang, K. Sun, Y. Xing, L. Feng, and H. Ge, "A modular grid-connected photovoltaic generation system based on dc bus," *IEEE Transactions on Power Electronics*, vol. 26, no. 2, pp. 523–531, 2011.

[3] S. Vighetti, J. Ferrieux, and Y. Lembeye, "Optimization and design of a cascaded dc/dc converter devoted to grid-connected photovoltaic systems," *IEEE Transactions on Power Electronics*, vol. 27, no. 4, pp. 2018–2027, 2012.

[4] V. M. Iyer, S. Gulur, G. Gohil, and S. Bhattacharya, "An approach towards extreme fast charging station power delivery for electric vehicles with partial power processing," *IEEE Transactions on Industrial Electronics*, vol. 67, no. 10, pp. 8076–8087, 2020.

[5] M. S. Agamy, D. Dong, L. J. Garcés, Y. Zhang, M. E. Dame, X. Wu, and Y. Pan, "A high power medium voltage resonant dual active bridge for mvdc ship power networks," *IEEE Journal of Emerging and Selected Topics in Power Electronics*, vol. 5, no. 1, pp. 88–99, 2017.

[6] R. Soman, M. M. Steurer, T. A. Toshon, M. O. Faruque, and R. M. Cuzner, "Size and weight computation of mvdc power equipment in architectures developed using the smart ship systems design environment," *IEEE Journal of Emerging and Selected Topics in Power Electronics*, vol. 5, no. 1, pp. 40–50, 2017.

[7] G. L. Kusic, G. F. Reed, J. Svensson, and Z. Wang, "A case for medium voltage dc for distribution circuit applications," in *2011 IEEE/PES Power Systems Conference and Exposition*, 2011, pp. 1–7.

[8] A. Hinz, M. Stieneker, and R. W. De Doncker, "Impact and opportunities of medium-voltage dc grids in urban railway systems," in *2016 18th European Conference on Power Electronics and Applications (EPE'16 ECCE Europe)*, 2016, pp. 1–10.

[9] M. Mogorovic and D. Dujic, "Fem-based statistical data-driven modeling approach for mft design optimization," *IEEE Transactions on Power Electronics*, vol. 35, no. 10, pp. 10 863–10 872, 2020.

[10] S. P. Engel, N. Soltau, and R. W. De Doncker, "Instantaneous current control for the three-phase dual-active bridge dc-dc converter," in *2012 IEEE Energy Conversion Congress and Exposition (ECCE)*, 2012, pp. 3964–3969.

[11] A. Marzoughi, R. Burgos, and D. Boroyevich, "Investigating impact of emerging medium-voltage sic mosfets on medium-voltage high-power industrial motor drives," *IEEE Journal of Emerging and Selected Topics in Power Electronics*, vol. 7, no. 2, pp. 1371–1387, 2019.

[12] L. Wang, Q. Zhu, W. Yu, and A. Q. Huang, "A medium-voltage medium-frequency isolated dcdc converter based on 15-kv sic mosfets," *IEEE Journal of Emerging and Selected Topics in Power Electronics*, vol. 5, no. 1, pp. 100–109, 2017.

[13] Z. Lu, C. Li, A. Zhu, H. Luo, C. Li, W. Li, and X. He, "Medium voltage soft-switching dc/dc converter with series-connected sic mosfets," *IEEE Transactions on Power Electronics*, vol. 36, no. 2, pp. 1451–1462, 2021.

[14] J. Hu, P. Joebges, G. C. Pasupuleti, N. R. Averous, and R. W. De Doncker, "A maximum-output-power-point-tracking-controlled dual-active bridge converter for photovoltaic energy integration into mvdc grids," *IEEE Transactions on Energy Conversion*, vol. 34, no. 1, pp. 170–180, 2019.

[15] D. Dujic, G. K. Steinke, M. Bellini, M. Rahimo, L. Storasta, and J. K. Steinke, "Characterization of 6.5 kv igbts for high-power medium-frequency soft-switched applications," *IEEE Transactions on Power Electronics*, vol. 29, no. 2, pp. 906–919, 2014.

[16] A. K. Tripathi, K. Mainali, D. C. Patel, A. Kadavelugu, S. Hazra, S. Bhattacharya, and K. Hatua, "Design considerations of a 15-kv sic igbt-based medium-voltage high-frequency isolated dcdc converter," *IEEE Transactions on Industry Applications*, vol. 51, no. 4, pp. 3284–3294, 2015.

[17] G. Ortiz, H. Uemura, D. Bortis, J. W. Kolar, and O. Apeldoorn, "Modeling of soft-switching losses of igbts in high-power high-efficiency dual-active-bridge dc/dc converters," *IEEE Transactions on Electron Devices*, vol. 60, no. 2, pp. 587–597, 2013.

[18] D. Dujic, S. Lewdeni-Schmid, A. Mester, C. Zhao, M. Weiss, J. Steinke, M. Pellerin, and T. Chaudhuri, "Experimental characterization of llc resonant dc/dc converter for medium voltage applications," in *International Power Conversion and Intelligent Motion Conference PCIM; May 1719, 2011, Nürnberg, Germany,*, 2011, pp. 265–271.

[19] S. Bernet, "Recent developments of high power converters for industry and traction applications," *IEEE Transactions on Power Electronics*, vol. 15, no. 6, pp. 1102–1117, 2000.

[20] H. F. Bilgin, M. Ermis, K. N. Kose, A. Cetin, I. Cadirci, A. Acik, T. Demirci, A. Terciyanli, C. Kocak, and M. Yorukoglu, "Reactive-power compensation of coal mining excavators by using a new-generation statcom," *IEEE Transactions on Industry Applications*, vol. 43, no. 1, pp. 97–110, 2007.

[21] Y. Suh and P. K. Steimer, "Application of igct in high-power rectifiers," *IEEE Transactions on Industry Applications*, vol. 45, no. 5, pp. 1628–1636, 2009.

[22] A. V. Rocha, H. de Paula, M. E. dos Santos, and B. J. Cardoso Filho, "A thermal management approach to fault-resilient design of three-level igct-based npc converters," *IEEE Transactions on Industry Applications*, vol. 49, no. 6, pp. 2684–2691, 2013.

[23] D. Andler, R. Álvarez, S. Bernet, and J. Rodríguez, "Experimental investigation of the commutations of a 3l-anpc phase leg using 4.5-kv5.5-ka igcts," *IEEE Transactions on Industrial Electronics*, vol. 60, no. 11, pp. 4820–4830, 2013.

[24] D. Stamenkovic, "Igct based solid state resonant conversion," EPFL, Thesis number 7843, Tech. Rep., 2020.

[25] J. Kucka and D. Dujic, "Smooth power direction transition of a bidirectional llc resonant converter for dc transformer applications," *IEEE Transactions on Power Electronics*, vol. 36, no. 6, pp. 6265–6275, 2021.

[26] D. Stamenkovic, U. R. Vemulapati, T. Stiasny, M. Rahimo, and D. Duji, "Igct low-current switchingtcad and experimental characterization," *IEEE Transactions on Industrial Electronics*, vol. 67, no. 8, pp. 6302–6311, 2020.

Gabriele Ulissi (S18) received the B.Sc. degree in electrical engineering from the Polytechnic of Turin, Italy, in 2016 and M.Sc. degree in electrical engineering from the École Polytechnique Fédérale de Lausanne (EPFL), Switzerland, in 2018. Since 2018, he is a Doctoral Assistant with the Power Electronics Laboratory at École Polytechnique Fédérale de Lausanne (EPFL), Switzerland. His research focuses on semiconductor-based protection of dc systems and dc transformers.

Jakub Kucka (Member, IEEE) received the bachelors and masters degrees in electrical engineering from Czech Technical University, Prague, Czech Republic, in 2012 and 2014, respectively, and the Dr.-Ing. (Ph.D.) degree from Leibniz University Hannover, Hanover, Germany, in 2019. From 2014 to 2019, he was a Research Associate with the Institute for Drive Systems and Power Electronics, Leibniz University Hannover. After, he was a Postdoctoral Researcher with the Power Electronics Laboratory, EPFL, Lausanne, Switzerland until November 2021. Since then, he has been with Large Drives Applications, Siemens AG. He has authored more than 20 scientific publications, one tutorial, and filed five patent applications. His research interests include modular multilevel converters, converter control and design, and resonant converter topologies suitable for high-power dc applications. Dr. Kucka was the recipient of EPE Outstanding Young Member Award in 2020 and SEMIKRON Young Engineer Award in 2021.

Umamaheswara Reddy Vemulapati (M12) received the bachelors degree in electrical engineering from RGMCET affiliated to JNTU Hyderabad, India. He received the Masters degree and the Ph.D. degree in electrical engineering from the University of Bremen, Germany. He joined ABB Switzerland Ltd., Corporate Research in 2011. Since then he worked on high-power semiconductor devices, such as IGCTs, IGBTs and Fast Recovery Diodes. Currently he is a principal engineer at Hitachi Energy, Semiconductors, Switzerland.

Thomas Stiasny received the Diploma and Ph.D. degrees in physics from Friedrich-Alexander University, Erlangen, Germany, in 1991 and 1996, respectively. He joined ABB Semiconductors, Lenzburg, Switzerland in 1997. Areas of work were development of Bipolar semiconductors and reliability aspects of those. Currently he is a senior principal engineer at Hitachi Energy, Semiconductors, Switzerland.

Drazen Dujic (S03-M09-SM12) received the Dipl.-Ing. and M.Sc. degrees from the University of Novi Sad, Novi Sad, Serbia, in 2002 and 2005, respectively, and the Ph.D. degree from Liverpool John Moores University, Liverpool, U.K., in 2008, all in electrical engineering. From 2002 to 2006, he was with the Department of Electrical Engineering, University of Novi Sad, as a Research Assistant. From 2006 to 2009, he was with Liverpool John Moores University, as a Research Associate. From 2009 to 2013, he was with the ABB Corporate Research Centre, Switzerland, as the Principal Scientist, working on the power electronics projects spanning the range from low-voltage/power SMPS in below kilowatt range to medium voltage high-power converters in a megawatt range. From 2010 to 2011, he was a member of a project team responsible for the development of the worlds first power electronic traction transformer successfully commissioned on the locomotive. From 2013 to 2014, he was with ABB Medium Voltage Drives, Turgi, Switzerland, as a Research and Development Platform Manager, responsible for ABBs largest IGCT-based medium voltage drive ACS6000. He is currently with the École Polytechnique Fédérale de Lausanne (EPFL), Lausanne, Switzerland, as an Associate Professor and the Director of the Power Electronics Laboratory. He has authored or coauthored more than 200 scientific publications and has led 18 patents. His current research interests include the areas of design and control of advanced high-power electronics systems for medium voltage applications. He has received the First Prize Paper Award from the Electric Machines Committee of the IEEE Industrial Electronics Society, in 2007. In 2014, he has received the Isao Takahashi Power Electronics Award for outstanding achievement in power electronics, and in 2018, the EPE Outstanding Service Award from the European Power Electronics and Drives Association. He is an Associate Editor of the IEEE TRANSACTIONS ON INDUSTRIAL ELECTRONICS, the IEEE TRANSACTIONS ON POWER ELECTRONICS, and the IET Electric Power Applications.